J. Fluid Mech. (1993), *vol.* 249, *pp.* 73–97

An incompressible jet in a weak crossflow

By F. J. HIGUERA[1] AND MANUEL MARTÍNEZ[2]

[1] E. T. S. Ingenieros Aeronáuticos, Pza. Cardenal Cisneros 3, 28040 Madrid, Spain

[2] Department of Aeronautics and Astronautics, MIT, Cambridge, MA 02139, USA

(Received 14 October 1991 and in revised form 23 July 1992)

A description of the incipient bending of a round incompressible jet issuing into a weak crossflow is presented. Axial vorticity is shown to appear from the early stages of the jet evolution owing to the distortion and reorientation of the azimuthal vorticity, and it eventually dominates the flow around the jet and determines the shape of its cross-section.

The crossflow is considered weak enough for the distortion of the jet to occur downstream of its development region, where diffusion already influences the whole cross-section and the jet can be modelled as a point source of momentum. Axial pressure gradient and axial diffusion are negligible under these conditions, since the jet is a slender structure.

Sufficiently near the origin, a finite-length entraining wake is identified on the lee side of the jet, which gradually merges with the main core. At the same time, the cross-section begins to acquire a characteristic elongated shape, with the jet concentrating in a thin layer. Farther downstream the axial vorticity of the jet rearranges into a couple of large locally two-dimensional contrarotating vortices standing against the wind under the action of their own induced velocity, and a smaller vortex sheet coinciding with the distorted jet.

1. Introduction

Observation of a strong jet issuing into a weak uniform transverse wind shows that the jet cross-section changes from circular to kidney-shaped and that two contra-rotating vortices parallel to the jet appear on its lee side, which gradually dominate the dynamics of the surrounding fluid. At the same time the jet begins to bend in the direction of the wind.

Early research focused on the empirical description of global features of turbulent jets, mainly the jet path (Jordinson 1958; Keffer & Baines 1963; Pratte & Baines 1967). Kamotani & Greber (1972) measured, in addition to the jet path, cross-sectional mean velocity distributions over a wide range of jet-to-wind velocity ratios. They pointed out the presence of a vortex pair deforming the cross-section and even shifting the location of the maximum velocity from the symmetry plane toward the centres of the vortices. Also, from their measurements, they suggested that the turbulent entrainment is nearly independently controlled by the components of the wind velocity normal and parallel to the jet. Placing particular emphasis on the vortex structure, Fearn & Weston (1974) described the flow transverse to the jet as the superposition of the uniform wind and a couple of locally straight vortices whose position, size, and strength were determined from the measured velocity field.

Integral models are the first semi-empirical tool used in the analysis of these flows. They give the evolution of global quantities along the jet by applying conservation equations is integral form, and require definite assumptions on the cross-sectional

shape and velocity profiles, entrainment rate, and surface forces. Differences among the models arise in the representation of these features. For example, the model of Sucec & Bowley (1976), as well as some earlier models, does not specify an entrainment rate; instead the rate of expansion of the jet boundary is prescribed as an empirical relation. In this model, and in those of Vizel & Mostinskii (1965) and Endo (1974) among others, the deflection of the jet is attributed to the pressure drag, and the momentum supplied by the entrained fluid is neglected. Examples of exactly the opposite assumption are the models of Platten & Keffer (1968) and Hoult & Weil (1972), while more sophisticated models include both effects. The success of an integral model is typically measured by its ability to predict the jet trajectory and size. However, these predictions seem to depend not only on the physical assumptions involved in the formulation of the model, but also on the tuning of the functions and coefficients used to represent the physical processes. It appears that there are many even contradictory combinations of physical assumptions leading to reasonable results and, as a consequence, integral models are of very limited value to elucidate the mechanics of the flow.

A number of models have been proposed that also predict details of the flow field. Adler & Baron (1979) were able to predict the development of a kidney-shaped cross-section by considering the evolution of a two-dimensional vortex sheet along the boundaries of the jet and expressing the growth rate of the cross-section as the sum of that of a turbulent jet in stagnant fluid and a contribution due to a vortex pair. The idea that a three-dimensional vortex sheet can be approximated by a two-dimensional one evolving in time dates back to Chen (1942). However, Coelho & Hunt (1989) showed that the approximation is fundamentally incorrect because it leaves out the interplay between axial and transverse vorticity components, which is an important element of the real three-dimensional flow. The model of LeGrives (1978) includes a locally two-dimensional vortex pair slightly behind the jet trajectory, whose characteristics and the entrainment rate they induce are evaluated using vortex dynamics laws and a correspondence with another model based on pressure drag. Karagozian (1986) models the jet as a couple of contra-rotating Rankine vortices moving, together with the surrounding fluid, under the action of forces induced on one another. The cores of the vortices grow due to turbulent diffusion and their strength is given by an empirical relation in terms of the flow impulse and the vorticity associated to the shear of the wind on the lateral boundary of the jet. All these models contain empirical elements supported, at best, by plausibility arguments or by consistency with the basic conservation laws.

Many inviscid analyses exist, beginning with the work of Chen (1942), which describe the effect of the wind in the potential core of the jet and retain a qualitative value farther downstream. A definite assessment of what aspects of the real flow can be understood independently of the viscosity or the modelling of Reynolds stresses is provided by the works of Needham, Riley & Smith (1988), Coelho & Hunt, and Needham *et al.* (1990). They consider an inviscid three-dimensional vortex sheet model for the near field of a jet with high jet-to-wind velocity ratio (the jet issuing from an orifice in a plate in the work of Coelho & Hunt, and from a semi-infinite pipe in that of Needham *et al.*). The inviscid models demonstrate that the distortion of the main azimuthal vorticity, with generation of additional axial and transverse vorticity, has already begun in the interior of the pipe. However, they also predict an unrealistic symmetric deformation of the cross-section outside the pipe and no overall deflection of the jet in the direction of the wind when the wind and the issuing jet are strictly perpendicular. The analysis of Needham *et al.* predicts a deflection of

the jet when there is a co-flowing component of the velocity external to the jet. Coelho & Hunt were able to restore this important feature by modelling the jet as an entraining vortex sheet, with an entrainment rate proportional to the velocity jump across the sheet.

More detailed predictive methods for developed turbulent jets should rely on numerical solutions of the relevant conservation equations. However, direct numerical simulation of this problem involves strong computer requirements, specially for large jet-to-wind velocity ratios for which the evolution of the jet spans large regions. As a consequence, a variety of numerical techniques has been tried in conjunction with different closure models, ranging from a constant turbulent viscosity in early work (e.g. Chien & Schetz 1975) to the routine use of k–ϵ models in more recent studies (after e.g. Patankar, Basu & Alpay 1977 and Demuren 1983).

This paper deals with the first stages of the bending of a jet in a weak cross-wind. The first important effect of the weak wind occurs when the radial velocity inside the jet, much smaller than the axial one, becomes comparable to the wind velocity. Since, in the absence of any wind, the velocity in the interior of a fully developed jet would decay as the inverse of the distance to the jet origin, the condition above defines the characteristic length of a distortion region where the transverse structure of the jet is strongly modified by the wind and its cross-section ceases to be circular. For the present purposes, the wind will be considered weak if the distortion region is long compared with the development region of the jet. Our goal is to describe the flow in that distortion region under these conditions.

The most prominent feature of this flow is the appearance of axial vorticity, which arises from the reorientation of the main azimuthal component and very soon becomes an essential element of the dynamics. Another characteristic feature is that the axial velocity remains large compared to the transverse velocity and therefore the deflection of the jet is small. Still another feature, associated to the slenderness of the jet, is that the axial pressure gradient and the axial diffusion are negligible and the conservation equations become parabolic in the direction of the jet. The analysis of the distortion region describes only the initial stages of the bending process. However, the asymptotic results obtained for the shape of the cross-section and for the distribution of vorticity give a clue to what the subsequent evolution may be.

The analysis is applicable to laminar jets and, in a more qualitative sense, to the mean flow of turbulent jets, if the simple mixing-length model with constant eddy viscosity is considered an acceptable approximation. Certainly, this is not the case in the development region, nor it is true for low jet-to-wind velocity ratios, for which most of the evolution occurs within a short distance from the outlet. Furthermore, as the jet deflects appreciably, the eddy viscosity distribution changes. Nevertheless, the constant-eddy-viscosity model gives quite acceptable results for the mean flow of a fully developed turbulent jet in the absence of crossflow, and, in a sense, when the distortion of the cross-section is moderate and evolves smoothly, the flow we consider is a perturbation of that flow. On this basis, we expect the results of the constant-viscosity model to retain at least a qualitative meaning for turbulent jets, in the nature of an analogy. The above justification breaks down far from the origin, but by then, as we shall see, the effect of turbulent diffusion is confined to a narrow strip, and new relevant length and velocity scales can be identified, leading to a new turbulent viscosity with which the qualitative description can be continued somewhat farther downstream.

While it is a rather extreme case, the limit of weak cross-wind is amenable to a fairly general analysis, which is not possible for moderate or small jet-to-wind

velocity ratios, of greater practical interest. Thus, among the large amount of work devoted to these latter cases, Moussa, Trischka & Eskinazi (1977) and Andreopoulos (1982) measured the velocity, jet contours, and turbulence intensity near the jet exit, pointing out the important role that the geometrical configuration of the boundaries and the velocity profile inside the pipe play in the mixing and development process. Sykes, Lewellen & Parker (1986) carried out a numerical simulation of the three-dimensional mean flow of a round turbulent jet with a low velocity ratio, showing that turbulent diffusion smears out the azimuthal vorticity in the fore and aft regions of the jet, and the vorticity left on the sides of the jet evolves very rapidly into an asymptotic far-field configuration without much vorticity reorientation.

2. Orders of magnitude and formulation

Consider first a round jet discharging with uniform velocity U_I from a circular orifice of diameter D_I into a space filled with stagnant fluid of the same density as the fluid in the jet. Assume that the Reynolds number $Re = U_I D_I/\nu$ is moderate enough for the flow to go through the development region, of length $O(Re\,D_I)$, before any instability had had time to grow to an appreciable size. After the development region, the flow attains the well-known Landau's self-similar solution for a point source of momentum (Batchelor 1967), dependent only on ν and the injected momentum flux $F = \frac{1}{4}\pi U_I^2 D_I^2$, which is conserved along the jet. For $\beta \equiv 8\nu/(3F/\pi)^{\frac{1}{2}} = 16/(\sqrt{3}Re) \ll 1$ (β being the angle at which the streamlines come closest to the axis), this solution is

$$w = \frac{8\nu}{\beta^2 z}\frac{1}{(1+\eta^2)^2}, \quad v_r = \frac{4\nu}{\beta z}\frac{\eta(1-\eta^2)}{(1+\eta^2)^2}. \tag{1}$$

Here $\eta = r/\beta z$, r is the distance to the axis of the jet, z is the distance along the axis, and v_r and w are the corresponding components of the velocity. Note that $v_r/w = O(\beta) \ll 1$ as a consequence of the slenderness of the jet. For a given z, the radial velocity is positive for $\eta < 1$, taking its maximum value $v_r = \nu/(\beta z)$ at $\eta \approx 0.414$, and negative for $\eta > 1$, taking its minimum value $v_r = -\nu/(\beta z)$ at $\eta \approx 2.414$. For $\eta \gg 1$ $v_r = -4\nu/(\beta z \eta) = -4\nu/r$, which is the velocity field of a two-dimensional sink. The jet entrains outer fluid that is accelerated vertically at the expense of the momentum of the interior fluid. The total entrainment rate is $m_e = -\lim_{r\to\infty} 2\pi r v_r = 8\pi\nu$, independent of z.

For a turbulent jet, the development region is about six diameters long and the fully developed jet is a cone of small angle, $2\beta \approx 10.5°$, determined experimentally. On dimensional grounds, the mean velocity of the fully developed jet is of the form $\boldsymbol{V} \equiv (v_r, w) = (F^{\frac{1}{2}}/z)\boldsymbol{f}(r/z)$, while, writing the Reynolds shear stress in the form $\overline{v_r' w'} = \nu_t \partial w/\partial r$, the turbulent viscosity must be $\nu_t = F^{\frac{1}{2}} h(r/z)$. The simplest closure, giving reasonable results for the mean flow, is to assume a constant ν_t. Then (1) holds for the mean velocity with ν_t playing the role of the viscosity, and the above relation between β and ν_t yields

$$\nu_t = \left(\frac{3F}{\pi}\right)^{\frac{1}{2}}\frac{\beta}{8} \approx 0.01 U_I D_I. \tag{2}$$

Let us consider now a jet discharging into a uniform stream of velocity $U_W \ll U_I$ perpendicular to the initial direction of the jet. This transverse stream will influence the flow in the core of the jet at heights such that its velocity and the maximum radial velocity induced by the jet in the absence of cross-wind are comparable.

Assuming that $\alpha \equiv U_I/U_W$ is sufficiently large, this will happen in the region of developed flow (where (1) holds and $v_r \sim 4\nu/\beta z$), at a height

$$z = O(4z_w), \quad \text{with} \quad z_w = (\sqrt{3}/16)\,\alpha D_I, \tag{3}$$

which defines the distortion region. Since $w/U_W = O(1/\beta) \gg 1$ in this region, the jet still moves in its initial direction with only a small deflection of order β. Also, the characteristic size of the cross-section is much smaller than z_w and the jet is a slender structure, although no longer axisymmetric. We note that the momentum flux F is the only feature of the discharging flow appearing in the distortion region. Hence, other (non-uniform) exit velocity profiles are acceptable as far as the distortion region is concerned, replacing the above value of F by the appropriate expression of the momentum flux and using $U_I \equiv (4F/\pi D_I^2)^{\frac{1}{2}}$ in the definition of α. This reflects the fact that, although the process of redistribution of the azimuthal vorticity in the development region of the jet depends on the exit velocity profile, the end result is still given by (1). We may also note that the radial jet velocity and the wind velocity do also become comparable below the distortion region for $r = O(\nu/U_w)$, but this corresponds to points outside the jet, while inside the jet the cross-wind is only a small perturbation to the axisymmetric solution (1). This two-region structure will be analysed in §3.

In the above scenario, the influence of the wind does not represent a drastic or abrupt change of the inner structure of the jet, but rather a cumulative perturbation whose effect appears in the 'long term'. In the application to turbulent jets, the expression (2) for the turbulent viscosity will be retained, as an approximation, in the distortion region. This is done on the grounds that (i) the flow has a well-defined main direction and does not differ drastically from an axisymmetric jet, and (ii) the gross features of the mean flow depend on factors other than an accurate modelling of the turbulence. None of these conditions is satisfied for lower jet-to-wind velocity ratios, and the analysis of those flows is far more complex than the present one. In particular, the possibility of studying the mean flow without a detailed analysis of the turbulence structure is lost. As mentioned in §1, the results of the present analysis are intended to be applicable to turbulent jets only in a qualitative sense.

For the estimate (3) to hold, $4z_w$ must be larger than the development region of the jet, which poses a lower bound to the velocity ratio ($\alpha > 15$ for a turbulent jet). This may be a strong restriction. For smaller values of α, which include many cases of practical interest, the distortion of the jet cross-section begins in the development region of the jet, and the analysis given below is not strictly applicable. However, the conclusions about the asymptotic behaviour for z/z_w large are probably valid.

The estimate (3) and the formulation that follows rely on the assumption that no instability of the initially circular jet grows to finite size over a distance shorter than $4z_w$. This condition restricts the range of applicability of the analysis for laminar flows, establishing bounds for the Reynolds number and the velocity ratio. A local linear stability analysis for parallel velocity profiles mimicking the development and fully developed regions (Morris 1976) shows that the flow in the development region becomes rapidly unstable, owing to the large vorticity concentration. Perturbations can grow downstream for Reynolds numbers above a critical value of the order of 10 and frequencies below a cutoff value varying like the inverse of the shear-layer thickness. The same trend holds for the fully developed flow (1), except that axisymmetric perturbations are linearly stable and the critical Reynolds number for helical perturbations is now about 37. When the slow divergence of the jet is accounted for (Crighton & Gaster 1976; Plaschko 1979), the growth rate of an

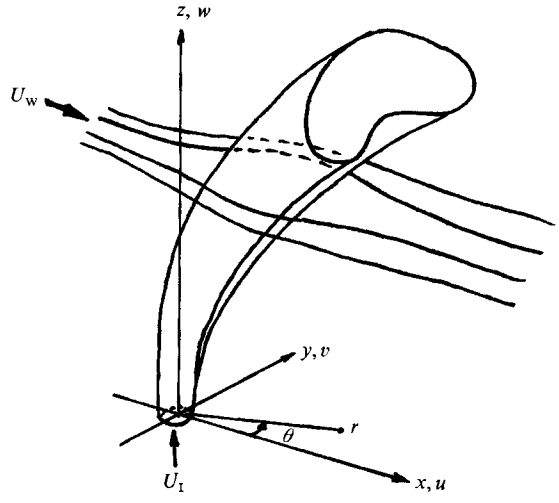

FIGURE 1. Definition sketch.

unstable perturbation of a given frequency is seen to first increase, then decrease, and finally become negative when progressing downstream. High-frequency perturbations have a large initial growth rate but they grow only during a shorter period than low-frequency perturbations, whereas there is a certain frequency for which the accumulated growth is maximum. On this basis, interference between the growth of the intrinsic instabilities of a laminar jet and the distortion due to the crossflow can be expected to be small for moderate Reynolds numbers and for a range of velocity ratios narrowing as the Reynolds number increases (to keep low both the growth rate and the accumulated growth).

Another magnitude of interest is the order of z corresponding to the bending of the jet, which occurs when w becomes comparable to the velocity of the wind. As we shall see in §§4 and 5, the analysis of the distortion region $[z = O(4z_w)]$ leads to the result that, asymptotically, w/U_W decays as $(z_w/z)^3/\beta$. Hence the bending becomes appreciable when $z = O(z_w/\beta^{\frac{1}{3}}) = O[\nu/(\beta^{\frac{1}{3}}U_W)]$. Note that typically this is not a long distance, and therefore the jet bends fairly rapidly, which makes more acceptable the stability condition of the previous paragraph.

Since our aim is to describe the flow in the distortion region, vertical distances in the remainder of the paper are referred to z_w, except where otherwise is stated explicitly. Horizontal distances are referred to βz_w, which is a measure of the jet cross-section, and the vertical (w) and horizontal (u, v) components of the velocity are referred to U_W/β and U_W, respectively. The pressure changes inside and around the jet will be referred to ρU_W^2, and the vertical component of the vorticity to $U_W/(\beta z_w)$. In terms of these dimensionless variables, which will be denoted by the same symbols used before for their dimensional counterparts, the continuity and momentum equations become

$$\nabla\cdot\boldsymbol{v}+\frac{\partial w}{\partial z}=0, \tag{4}$$

$$w\frac{\partial w}{\partial z}+\boldsymbol{v}\cdot\nabla w=\nabla^2 w+\beta^2\left(-\frac{\partial p}{\partial z}+\frac{\partial^2 w}{\partial z^2}\right), \tag{5}$$

$$w\frac{\partial \boldsymbol{v}}{\partial z}+\boldsymbol{v}\cdot\nabla\boldsymbol{v}=-\nabla p+\nabla^2\boldsymbol{v}+\beta^2\frac{\partial^2\boldsymbol{v}}{\partial z^2}, \tag{6}$$

where, with reference to figure 1,

$$\boldsymbol{x} = (x, y), \quad \boldsymbol{v} = (u, v), \quad \boldsymbol{\nabla} = (\partial/\partial x, \partial/\partial y), \quad \nabla^2 = \partial^2/\partial x^2 + \partial^2/\partial y^2,$$

The last terms of (5) and (6) will be dropped from this point onwards, being negligible for $\beta \ll 1$. We note that both the vertical pressure gradient and the vertical diffusion should be taken into account only for $(x, y) = O(z/\beta)$, because the structure of the flow is no longer slender in this remote region (which need not be analysed here).

Eliminating the pressure gradient between the two components of equation (6), the momentum equations (5)–(6) in the limit $\beta \to 0$ can be replaced by

$$w\frac{\partial w}{\partial z} + \boldsymbol{v}\cdot\boldsymbol{\nabla} w = \nabla^2 w, \tag{7}$$

$$\Omega = \frac{\partial v}{\partial x} - \frac{\partial u}{\partial y}, \tag{8}$$

$$w\frac{\partial \Omega}{\partial z} + \boldsymbol{v}\cdot\boldsymbol{\nabla}\Omega = \Omega\frac{\partial w}{\partial z} + \frac{\partial u}{\partial z}\frac{\partial w}{\partial y} - \frac{\partial v}{\partial z}\frac{\partial w}{\partial x} + \nabla^2\Omega, \tag{9}$$

where Ω is the vertical component of the vorticity.

The boundary conditions far from the jet are

$$u - 1 = v = w = \Omega = 0 \quad \text{for} \quad x \to \infty, \tag{10}$$

and the initial (in z) conditions can be written

$$(zu, zv, zw, z^2\Omega) \to (v_{rs}\cos\theta, v_{rs}\sin\theta, w_s, 0) \quad \text{for} \quad z \to 0, \tag{11}$$

where

$$w_s = \frac{8}{(1+\eta^2)^2}, \quad v_{rs} = \frac{4\eta(1-\eta^2)}{(1+\eta^2)^2}, \quad \eta = r/z. \tag{12}$$

These initial conditions express the fact that the effect of the wind becomes negligible and the self-similar solution (1) is recovered for $z \searrow 0$.

The limiting problem (4), (7)–(11), whose solution we address in the sequel, is free of parameters. This problem is closed and does not explicitly contain the pressure, which could be determined afterwards using (6) with $\beta = 0$.

3. Asymptotic solution for small z

In this section we describe the solution of (4), (7)–(11) for $z \ll 1$. This corresponds to the flow at heights above the origin of the jet larger than the length of the development region ($\alpha\beta z \gg 1$, leaving out numerical factors) but still small compared to the length of the distortion region. As mentioned before, two regions can be distinguished in this flow; an inner region coinciding with the core of the jet [$\eta = r/z = O(1)$; $z \ll 1$], where the effect of the wind amounts to a small perturbation of the self-similar solution (1), and an outer region [$r = O(1)$; $z \ll 1$], where the wind and the sink effect due to the entrainment of the jet dominate the transverse velocity field. A finite-length wake develops in this outer region. In what follows, the limit $\eta \to \infty$ in the inner region means $z \ll r \ll 1$, and the limit $r \to \infty$ in the outer region means $1 \ll r \ll z/\beta$.

Polar coordinates (r, θ) in the (x, y)-plane will be used in this section, with $\theta = 0$ pointing in the direction of the wind.

3.1. *Inner region*

The solution in the inner region can be written as a series expansion,

$$(w, v_r, v_\theta, z\Omega) = (1/z)\,(w^{(-1)}, v_r^{(-1)}, 0, 0) + (w^{(0)}, v_r^{(0)}, v_\theta^{(0)}, \Omega^{(0)}) + z(w^{(1)}, v_r^{(1)}, v_\theta^{(1)}, \Omega^{(1)}) + \ldots, \tag{13}$$

where the functions on the right-hand side depend on η and θ only. Writing (4), (7)–(11) in terms of η, θ, and z, inserting the expansions (13) in the resulting equations, and collecting terms of like order in z we would find in the first place equations for $w^{(-1)}$ and $v_r^{(-1)}$ whose solutions are given by (12). The next order yields a linear system of equations for $w^{(0)}$, $v_r^{(0)}$, $v_\theta^{(0)}$, and $\Omega^{(0)}$, whose coefficients are known functions of η. To cope with the boundary conditions (10), the solution of these equations must be of the form

$$(w^{(0)}, v_r^{(0)}) = \{Z(\eta), R(\eta)\}\cos\theta, \quad (v_\theta^{(0)}, \Omega^{(0)}) = \{\Phi(\eta), \Theta(\eta)\}\sin\theta, \tag{14}$$

where Z, R, Φ, and Θ satisfy the equations (the prime means derivative with respect to η)

$$-\eta^2 Z' + (\eta R)' + \Phi = 0, \tag{15}$$

$$-\frac{4\eta}{1+\eta^2}Z' - 8\frac{1-3\eta^2}{(1+\eta^2)^3}Z - \frac{32\eta}{(1+\eta^2)^3}R = \frac{(\eta Z')'}{\eta} - \frac{Z}{\eta^2}, \tag{16}$$

$$\eta\Theta = (\eta\Phi)' + R, \tag{17}$$

$$-\frac{4\eta}{1+\eta^2}\Theta' - \frac{32\eta^2}{(1+\eta^2)^3}(\Theta - \Phi') - 8\frac{1-3\eta^2}{(1+\eta^2)^3}Z = \frac{(\eta\Theta')'}{\eta} - \frac{\Theta}{\eta^2}, \tag{18}$$

with the boundary conditions

$$R - 1 = \Phi + 1 = Z = \Theta = 0 \quad \text{for} \quad \eta \to \infty, \tag{19}$$

and conditions of regularity at the origin ($\eta = 0$).

Out of the six linearly independent solutions of (15)–(18), only three are regular at the origin. For $\eta \gg 1$ two solutions are divergent, another behaves as

$$Z_1 \to 8/\eta^3, \quad R_1 \to 1 + O(\ln\eta/\eta^2), \quad \Phi_1 \to -1 + O(\ln\eta/\eta^2), \quad \Theta_1 = O(1/\eta^5), \tag{20}$$

matching with the lateral wind, and the other three solutions are

$$Z_2 = O(1/\eta^5), \quad R_2 \to a_2/\eta^2 + O(1/\eta^4), \quad \Phi_2 \to a_2/\eta^2 + O(1/\eta^4), \quad \Theta_2 = O(1/\eta^5), \tag{21}$$

$$Z_3 \to 4a_3/(\sqrt{5}+2)\,\eta^{\sqrt{5}+2}, \quad R_3 \to \sqrt{5}a_3/\eta^{\sqrt{5}+1}, \quad \Phi_3 \to a_3/\eta^{\sqrt{5}+1}, \quad \Theta_3 = O(1/\eta^{\sqrt{5}+4}), \tag{22}$$

and

$$Z_4 = O(1/\eta^{\sqrt{5}+4}), \quad R_4 \to a_4/\eta^{\sqrt{5}+1}, \quad \Phi_4 \to \sqrt{5}a_4/\eta^{\sqrt{5}+1}, \quad \Theta_4 \to -4a_4/\eta^{\sqrt{5}+2}. \tag{23}$$

The amplitudes a_2, a_3, and a_4 of these three modes were determined by a simple shooting method devised to kill the two diverging modes. The resulting profiles of Z, R, Φ and Θ are plotted in figure 2. These four functions, along with (14), describe the

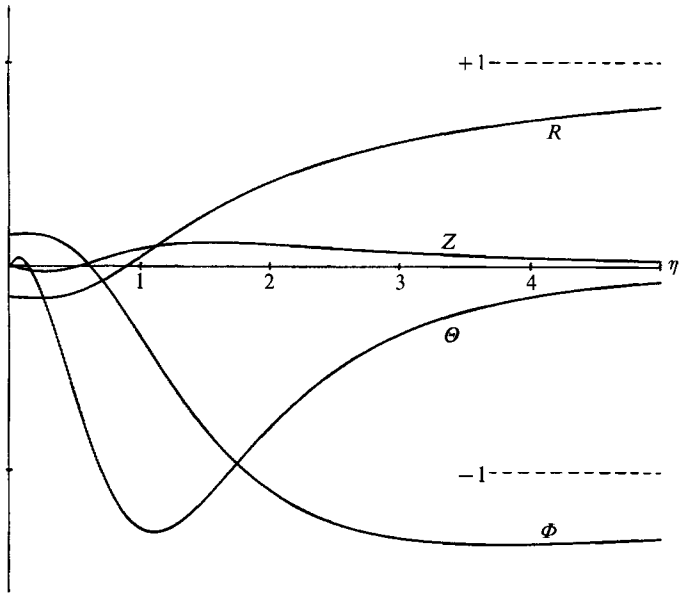

FIGURE 2. Solution in the inner region for small z. See (14).

main effect of the cross-wind on the core of the jet. The appearance of Z can be understood as a shift of the jet in the direction of the wind, whereas the negative sign of Θ in most of the places corresponds to the sense of rotation that one would expect from figure 1. Since axial vorticity is totally absent in the basic jet, $\Omega^{(0)}$ is a direct gauge of the effect of the cross-wind. The functions R and Φ, related to the horizontal velocity perturbation, decay more slowly than Z and Θ when moving away from the centre of the jet, mostly due to the mode (20). The signs of R and Φ in the outer part of the jet correspond loosely to the velocity perturbation that one would expect for a stream flowing around a solid body, but these signs are reversed for smaller η.

Going to the next order in the expansion (13) we would find

$$\left.\begin{aligned}(w^{(1)}, v_r^{(1)}) &= \{Z_{20}(\eta), R_{20}(\eta)\} + \{Z_{22}(\eta), R_{22}(\eta)\}\cos 2\theta \\ (v_\theta^{(1)}, \Omega^{(1)}) &= \{\Phi_{22}(\eta), \Theta_{22}(\eta)\}\sin 2\theta.\end{aligned}\right\} \tag{24}$$

We will not write down here the equations for all these functions. Suffice it to say that the behaviour of the axially symmetric parts of $w^{(1)}$ and $v_r^{(1)}$ are

$$Z_{20} \to 2/\eta^2, \quad R_{20} \to -8\ln\eta/\eta \quad \text{for} \quad \eta \to \infty. \tag{25}$$

R_{20} in particular gives the first non-zero correction to the jet entrainment rate

$$m_e = -z \lim_{\eta\to\infty} \int_0^{2\pi} \eta v_r \, \mathrm{d}\theta,$$

because all the other terms in (14) and (24) integrate to zero. The contribution of R_{20}, however, diverges as $16\pi z^2 \ln\eta$, reflecting the lack of uniform validity of the expansion (13).

3.2. *Outer region*

The radial velocity in (1) decays as $-4/z\eta$ for $\eta \to \infty$, becoming of the order of the wind velocity for $\eta = O(z^{-1})$, or $r = O(1)$. At the same time the asymptotic expansion for the axial velocity in (13) breaks down because the three first terms all become of

order z^3 (see (13), (14), (20), (24) and (25)). The appropriate expansions for the variables in the outer region $r = O(1)$, accounting for the matching conditions with the inner one, are

$$(w, v_r, v_\theta, \Omega) = (0, V_r^{(0)}, V_\theta^{(0)}, 0) + z^2\left(0, \frac{8\ln z}{r} + \frac{12\ln z}{r^2}\cos\theta + V_r^{(2)}, \frac{12\ln z}{r^2}\sin\theta + V_\theta^{(2)}, 0\right) + z^3(W^{(3)}, V_r^{(3)}, V_\theta^{(3)}, 0) + \ldots, \tag{26}$$

with

$$V_r^{(0)} = \cos\theta - 4/r, \quad V_\theta^{(0)} = -\sin\theta. \tag{27}$$

The vertical vorticity is of order $z^{\sqrt{5}+1}$ in the outer region, too small to influence the velocity field at order z^2, which is therefore irrotational. The logarithmic terms in (26) arise from the matching; see (20) and (25). Further logarithmic terms appear also at the next order (z^3), but these are not written explicitly; they can be considered as included into $V_r^{(3)}$ and $V_\theta^{(3)}$.

The variables $V_r^{(2)}$ and $V_\theta^{(2)}$ satisfy

$$(V_r^{(2)}, V_\theta^{(2)}) = \nabla\varphi, \quad \text{with} \quad \nabla^2\varphi = -3W^{(3)}, \tag{28}$$

whereas the leading order of the axial velocity satisfies the linear equation

$$\left(\cos\theta - \frac{4}{r}\right)\frac{\partial W^{(3)}}{\partial r} - \frac{\sin\theta}{r}\frac{\partial W^{(3)}}{\partial\theta} = \nabla^2 W^{(3)}, \tag{29}$$

with the boundary condition

$$W^{(3)} \to 0 \quad \text{for} \quad r \to \infty, \tag{30}$$

and the matching condition

$$W^{(3)} = g(r,\theta) + f + o(1) \quad \text{for} \quad r \to 0. \tag{31}$$

Here

$$g(r,\theta) = \frac{8}{r^4} + \frac{8\cos\theta}{r^3} + \frac{2(1+\cos 2\theta)}{r^2} + \frac{\cos\theta + \frac{1}{3}\cos 3\theta}{r} + \frac{1}{8} + \frac{\cos 2\theta}{6} + \frac{\cos 4\theta}{24}, \tag{32}$$

and f is an unknown constant that determines the flux of $W^{(3)}$ across any contour Γ enclosing the origin:

$$\phi = \oint_\Gamma (\boldsymbol{V}^{(0)} W^{(3)} - \nabla W^{(3)}) \cdot \boldsymbol{n}\, ds = -8\pi f. \tag{33}$$

We begin discussing the solution near the origin. The asymptotic expansion for $r \to 0$ or any even (in θ) solution of (29) begins as $r^{\lambda_n}\cos n\theta$, with $\lambda_n = -2 \pm (n^2+4)^{\frac{1}{2}}$ and n integer. Note that the first term of $g(r,\theta)$ in (31)–(32) corresponds to $n = 0$, ($\lambda_0 = 0, -4$), whereas the rest of $g(r,\theta)$ are the next four terms of the expansion of the solution beginning as $8/r^4$. These are computed straightforwardly from (29). Solutions with $n \neq 0$ and the minus sign in front of the square root are ruled out by the matching condition because they would diverge faster than $1/r^4$ for $r \to 0$. The companion solution with the plus sign in front of the square root may contribute to $W^{(3)}$ as an eigenfunction if it happens to go to zero for $r \to \infty$, which is unlikely in general. In any event, such a solution with $n \neq 0$ would give a zero flux across any circuit enclosing the origin and, therefore, only the solutions with $n = 0$ contribute to the flux (33). In our case, the coefficient of $1/r^4$ in (31)–(32) is already determined

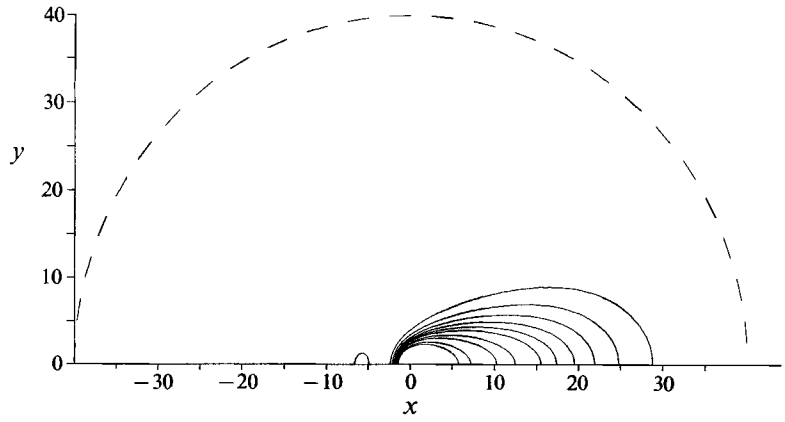

FIGURE 3. Contour lines of the vertical velocity in the outer region for small z.

by the matching condition and the flux can only be modified by acting on f. But, $W^{(3)} = f$ being an exact solution of (29), this freedom disappears when $W^{(3)}$ is forced to vanish at infinity, and the flux of $W^{(3)}$ is determined uniquely.

For $r \gg 1$ the effect of the sink is negligible and (29) becomes Oseen's equation in first approximation. $W^{(3)}$ decays exponentially to zero, except in a wake, $\zeta = \theta r^{\frac{1}{2}} = O(1)$, where the leading term of its asymptotic expansion is

$$W^{(3)} \sim a \frac{\zeta^{2m}}{r^{\frac{1}{2}+m}} \exp(-\zeta^2/4), \tag{34}$$

for some integer $m \geqslant 0$. Out of these possible behaviours, only the first one ($m = 0$) yields a flux different from zero, $\phi_{m=0} = 2\pi^{\frac{1}{2}}a$. Hence we must set $a = -4\pi^{\frac{1}{2}}f$.

Equations (29)–(31) were integrated numerically, yielding $a = 0.48$, $f = -0.068$. For the numerical integration, $W^{(3)}$ was decomposed as $W^{(3)} = W_S + W_R$, where $W_S = g(r,\theta)/(1+\kappa r^5)$, with $g(r,\theta)$ given by (32) and κ constant, is the singular part of the solution. W_R is then regular at the origin and vanishes at infinity. The equation for W_R was written in conservation form, discretized using centred finite differences, and solved with a pseudotransient method. The linear relation between W_R and $\partial W_R/\partial r$ that results from eliminating a between (34) and its first derivative was used as a far-field boundary condition.

Some isolines of $W^{(3)}$, revealing the shape of the solution, are plotted in figure 3. The overall structure of the flow, with the velocity field (27) due to a sink in a uniform stream and the wake (34) is in fair agreement with the flow visualizations of Werlé (1974, 1990), carried out for moderate values of r.

Vertical convection was neglected in (29) because $w\partial w/\partial z = O(z^5)$, whereas $\boldsymbol{v}\cdot\boldsymbol{\nabla} w = O(z^3)$ for $r = O(1)$. However, owing to the slow decay of $W^{(3)}$ in the wake ($w = O(z^3/r^{\frac{1}{2}})$ for $\zeta = O(1)$), both terms become of the same order when $r = O(z^{-4})$, $\zeta = O(1)$. This determines the limit of validity of the expansion (26), and in particular the termination of the wake where (34) holds, for vertical convection carries the material particles upwards before they have time to move horizontally over distances much larger than $O(z^{-4})$. Such a mechanism prevents an infinite wake. As a matter of fact no trace of the jet is left sufficiently far downstream for small values of z.

The termination of the wake could have been predicted on the grounds of internal consistency too. In fact, by integrating the continuity equation (4) over a large circle

of radius $R_\infty \gg 1$ with the velocity given by (26)–(28), we find that the mass flux entering the boundary of the circle increases with R_∞ as $6\pi^{\frac{1}{2}}az^2R_\infty$, due mainly to the entrainment of the wake. Such an entrainment rate would not be attainable if the wake extended down to infinity: there is no solution of (28) with $V_r^{(2)}$ and $V_\theta^{(2)}$ going to zero at infinity when $W^{(3)}$ is given by (34) with $m = 0$. (Actually the solution of (28) outside the wake is $\varphi = (3az^2/\pi^{\frac{1}{2}})\, r(\ln r \cos\theta - \theta \sin\theta)$ for $r \gg 1$). As a consequence, the flow required to feed an infinite wake would have to come from regions above and below the section where it is actually entrained, which is inconsistent with the approach leading to (4), (7)–(11).

Note that, for a turbulent jet, the result (34) depends on the assumption that the turbulent viscosity is constant. This assumption is about as reasonable for the wake as it was for the jet, for the product of the velocity (34) (decaying as $1/r^{\frac{1}{2}}$) and the width of the wake (growing as $r^{\frac{1}{2}}$) remains constant. Note also that if $a = 0$ the leading order of $W^{(3)}$ in the wake would have corresponded to $m \geqslant 1$ in (34), which leads to at most a logarithmically divergent entrainment. Then the expansions (26) would have been uniformly valid far downwind the jet.

Finally, for completeness, we sketch briefly the structure of the flow in the outermost region $[x = O(z^{-4}), y = O(z^{-2}), w = O(z^5)]$. The vertical momentum equation becomes

$$w\frac{\partial w}{\partial z} + \frac{\partial w}{\partial x} = \frac{\partial^2 w}{\partial y^2}, \tag{35}$$

and its solution is of the form $w = a^2z^5F(X, Y)$, with $X = a^2z^4x$, $Y = az^2y$, and

$$F\left(5F + 4X\frac{\partial F}{\partial X} + 2Y\frac{\partial F}{\partial Y}\right) + \frac{\partial F}{\partial X} = \frac{\partial^2 F}{\partial Y^2}, \tag{36}$$

$$F \to 0 \quad \text{for} \quad Y \to \pm\infty, \tag{37}$$

$$F = \exp(-Y^2/4X)/X^{\frac{1}{2}} \quad \text{for} \quad X \to 0. \tag{38}$$

The particle paths would be inclined straight lines in the absence of diffusion. Because of the effect of the diffusion in the y-direction these paths bend downwards near the symmetry plane of the jet and upwards outside. For large values of X the solution of (36) takes the form $F(X, Y) = G(p)/X$, where $p = Y/X^{\frac{1}{2}}$ and $G^2 - G + pG'/2 - G'' = 0$.

4. Numerical results

Continuing our analysis of (4), (7)–(11), we describe now the numerical solution in the bulk of the distortion region $[z = O(1)]$. For the purpose of the numerical computation, equation (8), defining the vorticity, is replaced by

$$\nabla^2 u = -\frac{\partial^2 w}{\partial x\, \partial z} - \frac{\partial \Omega}{\partial y}, \tag{39}$$

which is a combination of (4) and (8).

4.1. *Numerical method*

Equations (4), (7), (9)–(11) and (39) were solved for w, u, v, and Ω, with (7) and (9) written in conservation form. Only the half-space $y > 0$ was considered, with the symmetry conditions $v = \Omega = \partial w/\partial y = \partial u/\partial y = 0$ at $y = 0$ (one of them is redundant).

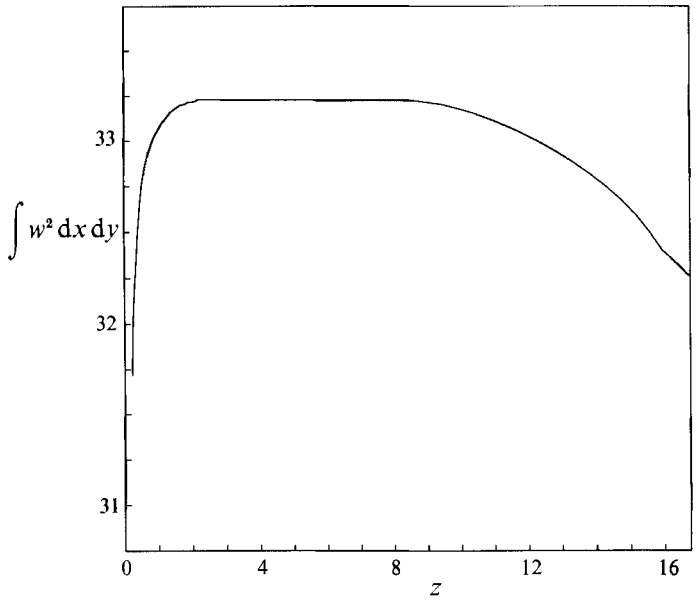

FIGURE 4. Numerically evaluated vertical momentum flux for half of the jet as a function of z.

Homogeneous Neumann conditions were applied for w and Ω at the outer boundaries of the computational domain, which was a rectangle in the (x, y)-plane. For u Dirichlet conditions were used upstream and Neumann conditions at the other boundaries. (For a more accurate treatment, the Poisson equation (39) was also approximately solved outside the computational domain using asymptotic wake-like expressions for w and Ω. This yields a relation between u and its normal derivative at the outer limit of the domain, which was used as a boundary condition for the solution inside the domain. However, this procedure required under-relaxed iteration, slowing down drastically the convergence rate.)

Initial conditions for the numerical integration are provided by the asymptotic solution of the previous section. The key elements of this solution affecting the evolution of the flow are the base self-similar velocity profiles, the axial vorticity induced by the wind inside the jet, and the uniform wind velocity outside.

The equations were discretized using finite volumes and a staggered grid, with an implicit (in z) centred representation for the x- and y-derivatives. The discrete problem was solved with a pseudotransient and ADI method for the vertical momentum and vorticity equations. One step of the artificial time involves: (i) a couple of ADI sweeps for (7) and (9) to update w and Ω, respectively; (ii) solution of the Poisson equation (39) for u by SIP iteration; (iii) direct integration of the continuity equation (4) to find v. These three stages were repeated cyclically until a converged stationary solution was achieved. Then z was advanced another step.

Since the size of the cross-section grows rapidly, we found it convenient to switch to the shifted and strained coordinates $(x-\gamma z^{\sigma})/z^{\tau}$ and y/z^{τ}, with piecewise constant γ, σ, and τ chosen to fit the grid to the evolving jet as closely as possible.

Figure 4 shows the total vertical momentum flux, $\int w^2\,dx\,dy$, which should be equal to $2^5\pi/3 \approx 33.51$, independent of z. This quantity was used as a test on the numerical computations performed with different grids, domain sizes, and implementations of the far-field boundary conditions. The low value of the momentum flux during the

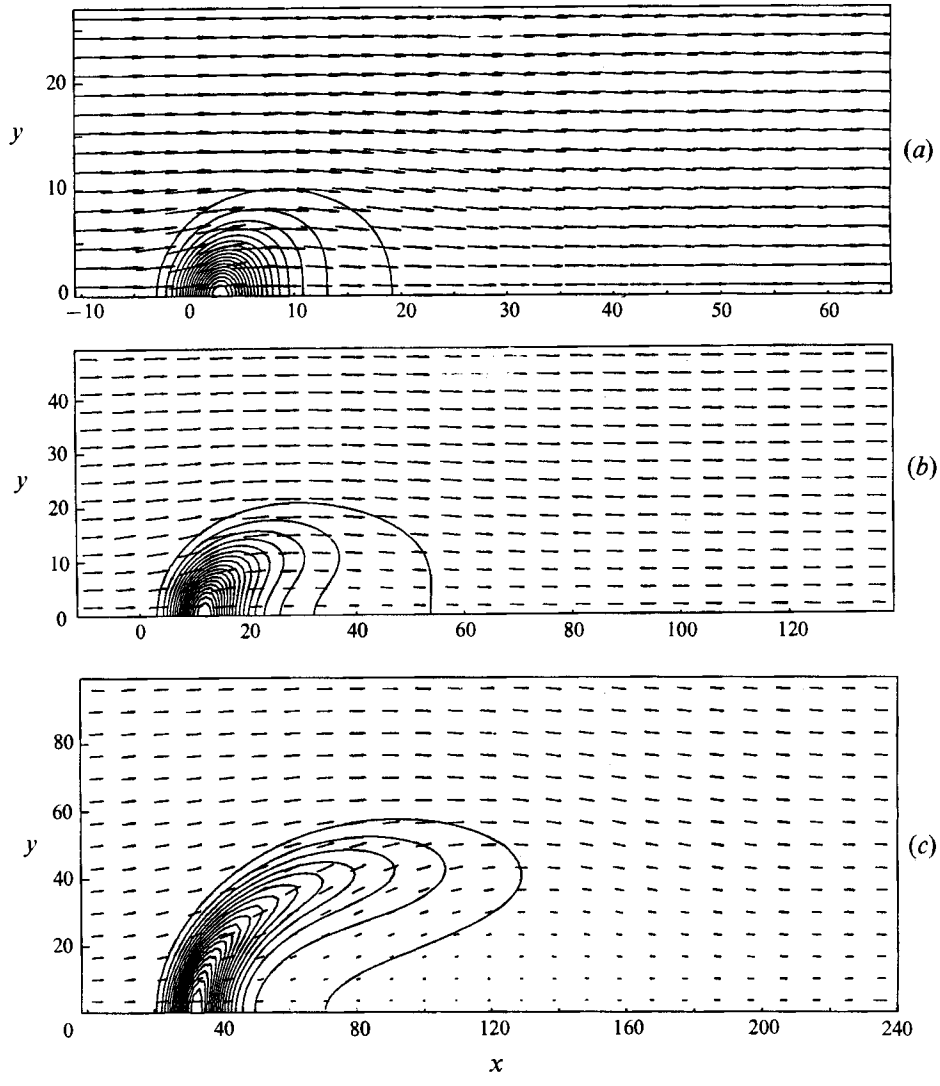

FIGURE 5. Contour lines of the vertical velocity and horizontal velocity arrows, for different horizontal sections. (*a*) $z = 5.20$: $0 \leqslant w \leqslant 1.43$; (*b*) $z = 9.85$: $0 \leqslant w \leqslant 0.70$; (*c*) $z = 15.73$: $0 \leqslant w \leqslant 0.33$. Equispaced lines.

early stages of the computation is partially an artifact introduced by the evaluation of this quantity from the numerical data when the size of the jet is very small and, more importantly, an effect of numerical diffusion, because the grid is comparatively coarse during these stages. The momentum flux decays again for large values of z owing to the finite size of the computational domain. This decay defines a limit beyond which the numerical results are no longer reliable. Another limit, related to the evolution of the vorticity, will be discussed in the next subsection.

4.2. *Results and discussion*

Figures 5 to 8 display results of the numerical computation for different values of z. In figure 5(*a–c*) isolines of the vertical velocity show the transition from the round growing jet for small z, where the entrainment flow is much stronger than the wind,

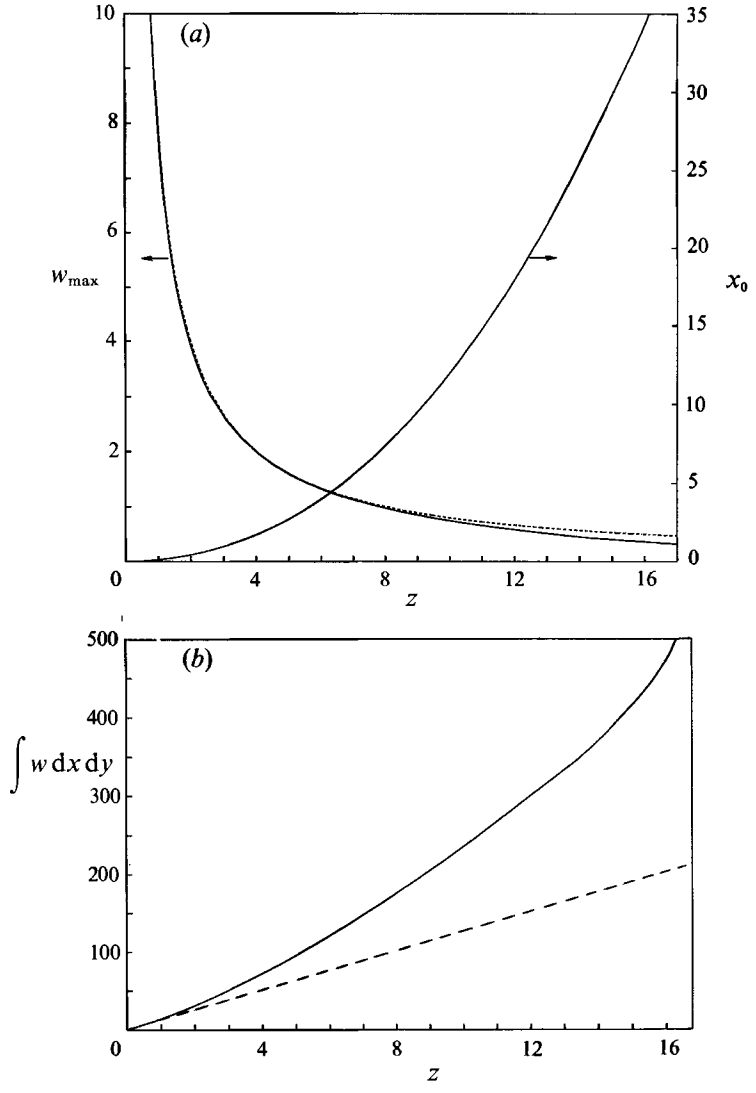

FIGURE 6. (*a*) Maximum vertical velocity and location of the maximum vertical velocity as functions of z. Dashed line represents the maximum vertical velocity for the axisymmetric jet. (*b*) Vertical mass flux for half of the jet as a function of z. Dashed line represents the mass flux for half of the axisymmetric jet.

to the characteristic kidney-shaped cross-section for larger z. The long ridge in figure 5(*c*) suggests that the jet cross-section is becoming a relatively narrow strip. The maximum axial velocity in each section is attained at a point $x_0(z)$ of the symmetry plane, defining the trajectory of the jet. Both $x_0(z)$ and the maximum velocity are represented in figure 6(*a*) as functions of z. For comparison, the dashed line in this figure represents the maximum vertical velocity for the axisymmetric solution (1) ($w_{max} = 8/z$ in non-dimensional terms). Figure 6(*b*) shows the mass flux for half of the jet, $\int w\,dx\,dy$, as a function of z. The dashed line ($4\pi z$) corresponds to the axisymmetric solution, the difference being $o(z^2)$ for $z \ll 1$, according to the results of §3. This quantity can be evaluated accurately only for moderate values of z, because an important contribution to the flux comes from far regions of the cross-section, which

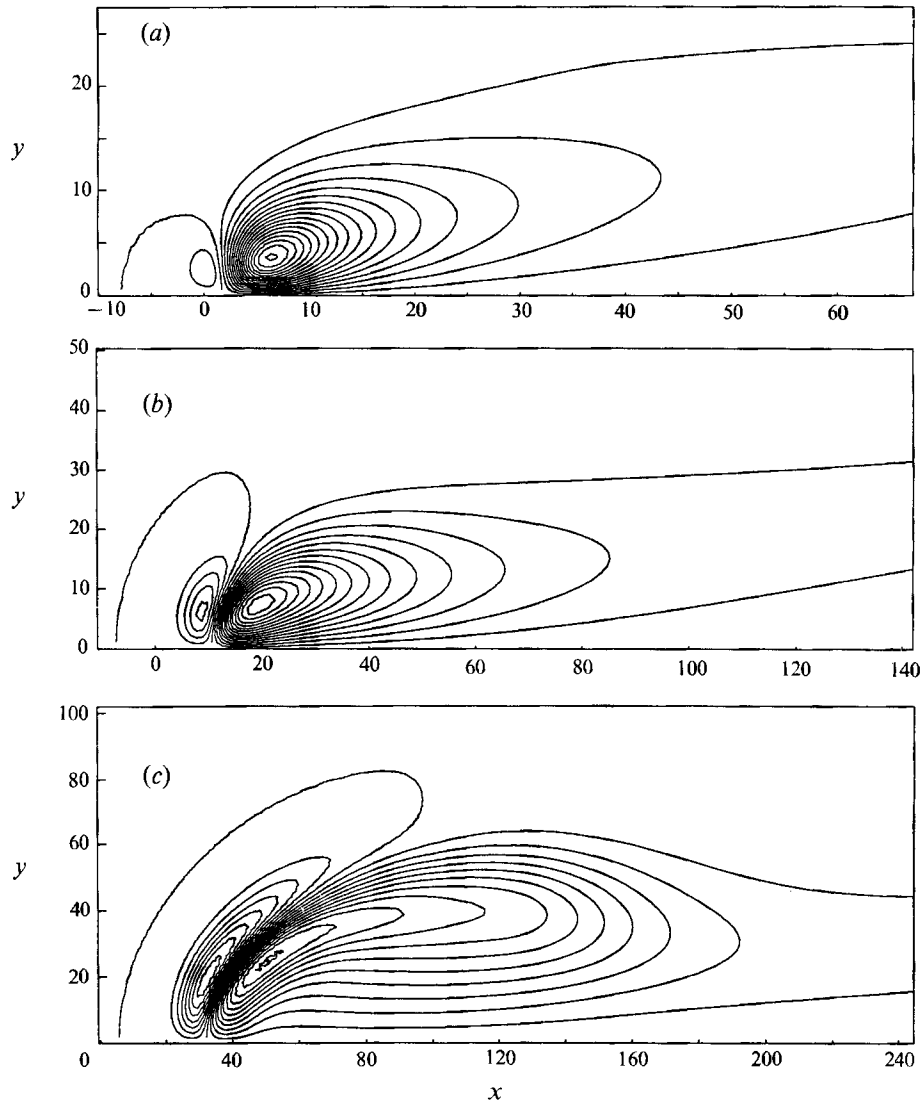

FIGURE 7. Contour lines of the vertical vorticity for different horizontal sections. (*a*) $z = 5.20$: $-0.234 \leqslant \Omega \leqslant 0.023$; (*b*) $z = 9.85$: $-0.168 \leqslant \Omega \leqslant 0.054$; (*c*) $z = 15.73$: $-0.111 \leqslant \Omega \leqslant 0.077$. Equispaced lines.

are affected by the finite size of the computational domain when z becomes large. On the basis of this limited information, the mass flux seems to increase at a rate consistent with the asymptotic description of the next section. Note that the entrainment rate is the derivative of the mass flux.

The arrows in figure 5 represent the horizontal components of the velocity. The effect of the entrainment is observable for moderate values of z. The apparent rate of expansion $(\partial u/\partial x + \partial v/\partial y)$ attains its largest negative values in the rear part of the jet, reflecting a high local entrainment rate. In the fore part the rate of expansion even becomes positive, but this must be attributed to the incipient inclination of the jet commented on below.

The signature of the vertical vorticity in figure 5 is more visible behind the jet, in

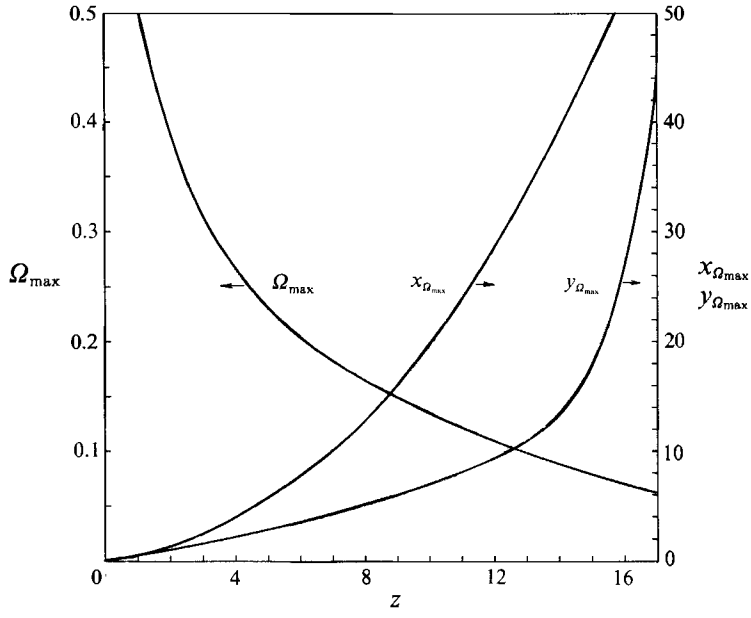

FIGURE 8. Maximum vertical vorticity and location of the maximum vertical vorticity as functions of z.

the region sheltered from the wind, and appears still more clearly in a plot of the velocity relative to the wind $(u-1, v)$ for moderate z (not presented), in which a recirculation region and a local velocity minimum are clearly visible at about the same location as the vorticity maximum depicted by the isolines of figure 7(*b*). The sheltering effect of the jet (i.e. of the region where $w \neq 0$) weakens as z increases, and the axial vortex pair gradually takes over in counteracting the wind.

Figure 7(*a–c*) shows the evolution of the vertical vorticity. The vorticity distribution is initially symmetric relative to the y-axis (see (14)) but very soon loses this symmetry and is convected by the wind. Vertical vorticity arises from the reorientation of the azimuthal component in the distorted jet and already exists in the early stages of the jet development. As the evolution proceeds, the vorticity begins concentrating in the same layer as the axial velocity, where it is generated. However, before long, a substantial amount of this vorticity is seen to leave the layer by the rear tips, leading to a couple of contrarotating vortices bigger than the jet and located behind it. Since the vertical velocity is negligible over most of the region occupied by the vortices, the motion there is two-dimensional and the vortices stand against the wind under the action of their own induced velocity.

The maximum value of the vorticity in the contrarotating vortices and its position are given in figure 8. As can be seen, the vortex pair grows very fast with increasing z, and the vortices hit the rear limit of the computational domain fairly soon, when the jet is still moderately small. It turns out that this is the strongest restriction on the values of z attainable numerically, for, from this point onwards, only a fraction of the vortices is left to offset the wind and the jet cross-section becomes artificially distorted as a consequence. This relatively clear failure of the numerical scheme proves the important role of the contrarotating vortices. Thus, computations carried out with a longer and narrower domain show a jet cross-section slightly more straight and aligned with the y-axis than that of figure 5(*c*).

Although the standing vortex pair is a prominent feature of this flow, it has also been reported (e.g. Moussa *et al.* 1977) that the stationary vortices may become unstable, giving rise to alternating shedding. In the present computation this possibility is precluded by the symmetry condition at the central plane. However the pseudotransient iteraction failed to converge in some cases for large values of z, and, in those cases, inspection of the vorticity field revealed large patches of vorticity moving downwind to the boundaries of the computational domain.

The deflection of the jet in a vertical plane begins to affect the appearance of the horizontal sections when z increases. The inclination angle, being still small, is sufficient for the axial velocity to have a horizontal component of the same order as the wind velocity, and for the vorticity normal to the jet direction to have a vertical component of the same order as the axial vorticity. These features are reflected in figures 5(*b*, *c*) and 7(*b*, *c*) by the presence of a large x-velocity in the central core of the jet and of a positive vertical vorticity (for $y > 0$) in the leading part of the jet wing. (Although, according to the interpretation given in the next section, not all the positive vorticity in figure 7*c* would be due to this effect.) As a consequence, some care is required to assess the axial vorticity distribution from inspection of figure 7, as the vorticity in the region occupied by the jet ($w \neq 0$) is contaminated by the aforesaid effect. Such cross-projection effects remain in the subsequent evolution of the jet, for the growth of the inclination angle and the decay of the axial velocity occur at the same pace. Cross-projection effects demonstrate, on the other hand, that the ascending motion of the fluid inside the jet and its horizontal shift by the action of the wind are equally important in the dynamics of the jet.

Additional computations were carried out with initial velocity profiles simulating the flow in the development region (Morris 1976) instead of the condition (11). For a laminar jet, this simple change extends the range of validity of the results to slightly lower velocity ratios, for which the distortion has already begun in the development region. (For a turbulent jet the model of constant eddy viscosity is inappropriate in the development region.) To the limited extent that these computations were carried out, the results show the same trends commented on before.

5. Asymptotic structure for large z

The numerical results of the previous section give no conclusive description of the asymptotic solution for $z \gg 1$. These results will be used now as a guide, in combination with order-of-magnitude estimates based on general properties of the conservation equations, to try to deduce as much information as possible about the nature of the asymptotic solution. For brevity, only an attempt at scaling is presented here, and two possible variations are briefly discussed in an Appendix. This section and the Appendix have a more qualitative character than the rest of the paper, and the methods applied here will not allow a decision among several apparently likely possibilities. Nevertheless, a reasonably complete description of the asymptotic state, which is crucial to the understanding of the key features of this flow, can be achieved by the present qualitative methods.

The former convection–diffusion balance of the axisymmetric jet, yielding transverse velocities of order $1/z$, clearly breaks down as z increases, for the horizontal wind acquires a growing influence and such a round jet would simply be swept away. As commented before, the jet develops axial vorticity in the form of two contrarotating vortices, and (backed by the results of the previous section and the

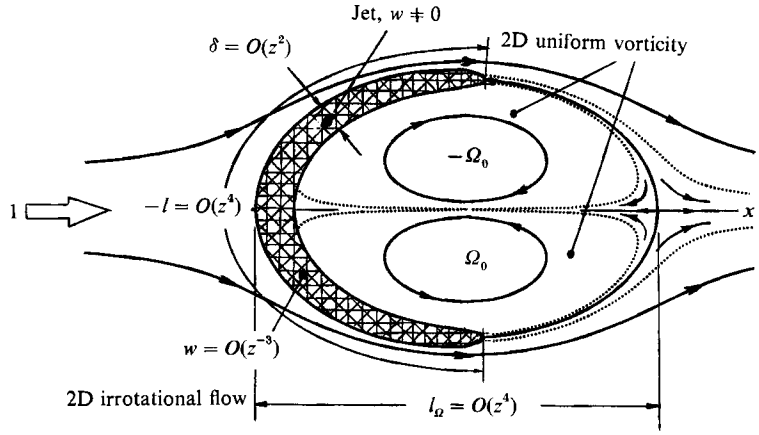

FIGURE 9. Sketch of the jet cross-section for large z.

extensive experimental evidence available) we may conjecture that a new balance sets in for large enough values of z, in which the horizontal velocity induced by the axial vorticity distribution counteracts the wind.

Defining the jet as the region where w is appreciably different from zero, figure 5(*c*) shows that the jet cross-section becomes an elongated strip for large values of z, which was to be expected as a result of the horizontal strain generated by the contrarotating vortices. Diffusion normal to this strip is the only mechanism left in (7) to counteract the straining, and it must therefore play a role in the dynamics.

Figure 9 is a sketch of the cross-section of the jet and the vortices for $z \gg 1$. We denote by l, δ, and w the characteristic (non-dimensional) values of the length and width of the jet cross-section and the vertical velocity, respectively. The way these quantities scale with z follows from the following considerations:

(i) The total vertical momentum flux is conserved along the jet. Hence $w^2 l\delta \sim 1$.

(ii) The fluid inside the jet moves horizontally (sidewise) with a velocity of order one (the wind velocity in non-dimensional variables) and vertically with a velocity of order w. Hence, the horizontal and vertical displacements after a time t verify the relations $l \sim t$ and $z \sim wt$, leading to $wl \sim z$.

(iii) Convection along the layer and diffusion across are both relevant to the flow inside the jet. Hence $\delta^2 \sim z/w$.

These three relations yield

$$l = O(z^4), \quad \delta = O(z^2), \quad w = O(1/z^3). \tag{40}$$

Let us consider now the axial vorticity distribution. The contrarotating vortex pair behind the jet (represented by the twin recirculating cells in figure 9) would extend over a length $l_\Omega = O(l)$, the jet itself being a narrow strip on the periphery of the vortices. Since the motion outside the jet is strictly two-dimensional, the vorticity should be uniform in each member of the pair ($\Omega = \mp\, \Omega_0 = O(z^{-4})$, say), which would then be one of the limiting members of the family of Batchelor–Prandtl vortices studied by Pierrehumbert (1980) (see Saffman & Tanveer 1982 for a correct description of this limiting flow), for which $\Omega_0 l_\Omega = 1.84$.

The vortices are continuously fed with vorticity coming from the jet, which makes up for the losses by diffusion through the outer boundary of the vortices and through the symmetry plane ($y = 0$ in figures 5 and 7). The dotted lines in figure 9 sketch the diffusion layers around the vortices and the beginning of the wake. Note that, from

the balance of production $[O(w/\delta z)]$ and convection $[O(w\Omega/z)]$ in (9), the peak vorticity is of order $1/z^2 \gg \Omega_0$ inside the jet (as clearly reflected in figure 7*c*). However, vorticity of both signs coexists here and the (horizontal) velocity jump across the sheet is only of order $1/z^2$, as we shall see below.

Another magnitude of interest is the overall downwind shift (x_0 in figure 6*a*). This can be estimated from the balance between the horizontal momentum entrained by the jet from its origin to the present height and the horizontal momentum flux crossing the normal cross-section of the jet, which is a reflection of the jet inclination. (Or, in other words, by establishing that the jet can sustain a continuous ingestion of horizontal momentum both because it is curved and has momentum flux along it.) Since the entrainment rate is $m_e = O(l\delta w/z) = O(z^2)$ (from the continuity equation) and the velocity outside the jet is of order one, the first quantity is of order z^3, whereas the second one is $O[w^2\delta l(x_0/z)]$. Hence

$$x_0 = O(z^4), \tag{41}$$

which is in good agreement with the experimental results of Kamotani & Greber (1972), and many others since then, on the trajectory of a turbulent jet in a cross-wind. The comparison, however, should be taken with caution, for the experimental results refer to the region of finite deflection of the jet.

The curvature of the jet in a vertical plane is of order x_0/z^2, leading to a pressure jump $\Delta p = O[w^2(x_0/z^2)\,\delta] = O(1/z^2)$ to counteract the 'centrifugal' force. This is also the order of the velocity jump across the sheet. The pressure drag, $O(\Delta p l) = O(z^2)$, is of the same order as the rate of entrainment of momentum estimated in the previous paragraph, and, therefore, both effects contribute to the bending of the jet.

Finally, consider the overall horizontal momentum balance for the flow outside the jet between two horizontal planes a unit distance apart. As can be easily verified, this balance states that the horizontal momentum imparted by the wind to the jet per unit length by both pressure drag and entrainment of momentum is equal to the sum of the horizontal momentum carried by the mass entrained by the jet per unit length when that mass moves with the velocity of the wind plus the defect of horizontal momentum in the wake. This latter term can be easily estimated because the velocity defect immediately downstream of the vortices (in the dotted region to the right of figure 9) is of the same order as the velocity jump across the jet ($1/z^2$) and the thickness of the wake is here of order δ. Hence, the defect of momentum is of order one, much smaller than the other terms in the overall balance mentioned above. We may also note that some vertical momentum is lost by the wake, which was not accounted for in (i) above. However, the very fact that this fluid departs from the main vertical stream indicates that its remaining vertical momentum is comparatively small. This loss of vertical momentum flux may contribute to the decay of $\int w^2\,\mathrm{d}x\,\mathrm{d}y$ observed in figure 4. Nevertheless, as commented on in §4, the main cause of the actual decay of the momentum flux in the computations for large z is thought to be the limited size of the computational domain, whose boundary is nearly hit by the growing jet, irrespective of the importance of the wake. This situation is difficult to avoid, given the fourth-power growth predicted by (40)–(41) for the size and the deflection of the jet.

Provided that a solution of this type exists, the angle of inclination of the jet to the vertical would become of order one when the axial velocity given by (40) decays to values of the order of the wind velocity (i.e. when $w = O(\beta)$ in non-dimensional terms). This happens for $z = O(1/\beta^{\frac{1}{3}})$, as was already advanced in §2, and, by then, both the downwind shift of the jet and the size of the vortices would be comparable

to the vertical distance from the origin (cf. the factor β^{-1} in the definition of the vertical length and velocity scales above (4)–(6)). At this point, the vortices would no longer be slender structures and the formulation of §2 breaks down.

The subsequent three-dimensional evolution ends up aligning the jet and the vortex pair with the free stream. Assuming that the flow in the far field is self-similar and that the only memory left of the injection conditions is the value of the momentum flux, Durando (1971) and Broadwell & Breidenthal (1984) conclude that the jet penetration distance and the vortex spacing vary in this region with the downstream distance raised to one third. Even though the transition to this terminal state may be very complex, the region of fully three-dimensional flow cannot be much larger than $z_w/\beta^{\frac{1}{3}}$, because the circulation of the vortices, built up during the two-dimensional stage, is not sufficient to keep the jet from bending once three-dimensional effects come into play.

For a turbulent jet, the assumption of constant eddy viscosity is the weakest point of this analysis. A more realistic assumption would perhaps be $\nu_t = O(w\delta)$. Introducing this expression into the estimates at the beginning of this section, we would find the modified scaling

$$l = O(z^3), \quad \delta = O(z), \quad w = O(1/z^2), \quad x_0 = O(z^3), \tag{42}$$

and $\nu_t = O(1/z)$. At any rate, neither these nor the scalings (40)–(41) are intended to be more than qualitative results. Our aim is to describe general features of the flow rather than the distributions of turbulent magnitudes. In this respect, we note that, since the only effect of the Reynolds stresses is to transfer momentum across the thin layer, the overall features (mainly the existence of the thin layer itself) might be relatively independent of how this transfer occurs.

6. Conclusions

The flow corresponding to the incipient bending of a jet under the action of a weak transverse wind is amenable to a simplified parameter-free formulation if the turbulent viscosity is assumed to be constant.

The asymptotic analysis of the early stages of the jet evolution, when the entrainment velocity inside the jet is still large compared with the wind velocity, shows that axial vorticity appears in the jet in the form of two contrarotating fore-and-aft-symmetric vortices growing linearly in size and strength along the jet. The increment of the jet entrainment rate due to the cross-wind grows roughly as the square of the distance along the jet during these early stages. In addition, a finite-length wake exists which is responsible for a larger entrainment. This wake shortens as the jet evolves, merging with the jet when its transverse velocity becomes comparable to the wind velocity.

The cross-section becomes appreciably distorted in the region where the transverse velocity of the jet and the velocity of the wind are of the same order. By then, the deflection of the jet is still small because the axial velocity is larger than the wind velocity. The equations describing the flow are solved numerically taking advantage of the simplifications due to the slenderness of the jet. The solution shows an incipient deflection of the jet in the direction of the wind. The cross-section grows and acquires an elongated shape, with axial vorticity concentrated inside and also spread over two larger contrarotating vortices outside the jet. Eventually this vorticity dominates the transverse motion outside the jet.

An order-of-magnitude analysis leads to an asymptotic description of this latter

stage in terms of an outer planar flow in cross-sectional planes, and an inner boundary-layer type of flow in the interior of the jet. The outer flow is driven by the vorticity concentrated in the large contrarotating vortices, which are fed with vorticity shed by the jet. The inner structure of the jet, determining the outflow of vorticity, depends in turn on the outer flow. The relative importance of pressure drag and entrainment of momentum is discussed.

We wish to thank A. Liñán for many invaluable discussions and advice.

Appendix. Alternative asymptotic models

In this appendix we set up the scalings for two possible variations of the asymptotic structure discussed in §5. As mentioned in the text, it seems that simple order-of-magnitude estimates do not suffice to decide what alternative is actually realized.

The idea that the jet is a thin layer extended on the periphery of the vortices is suggested by the appearance of figures 5(*c*) and 7(*c*). However, it might also happen that this layer rolls up at higher values of z, becoming a spiral inside the vortices, as sketched in figure 10(*a*). Here we discuss how the previous estimates should be modified in this case. The considerations (i)–(iii) leading to (40) still hold true. The size (l_Ω) of the vortices, however, becomes smaller than l in (40). To estimate this size we note first that the mean distance between turns of the spiral in figure 10(*a*) is of order l_Ω^2/l. Since the entrainment flux required to feed the jet ($m_e = O(z^2)$) must flow through the 'channels' left between adjacent turns, the velocity induced by the entrainment is of order $m_e/(l_\Omega^2/l)$. Further, we note that this velocity must be of the order of the wind velocity, for otherwise it would have no influence on the dynamics, and the recirculating flow inside the vortices would continuously increase the number of turns of the spiral (as if it were a passive surface), which is inconsistent with having a steady flow. Hence,

$$l_\Omega = O[(m_e\, l)^{\frac{1}{2}}] = O(z^3). \tag{A 1}$$

Using the scales (40), (41), and (A 1), the curvature radius of a typical streamline inside the jet (i.e. one completing at each height a number of turns comparable to the total number of turns of the spiral at that height) can be seen to be of order $1/z^3$, being due mainly to the rolling-up of the jet cross-section. The pressure jump across the sheet required to cope with the 'centrifugal' force associated to this curvature is $\Delta p = O(1/z)$, larger than that found in §5. This pressure jump could give a drag $O(\Delta p l) = O(z^3)$, much larger than the entrainment of horizontal momentum, and a downwind shift

$$x_0 = O(z^5). \tag{A 2}$$

(This large shift implies that the fluid inside the jet is moving horizontally much faster than the wind, as a consequence of the inclination of the jet.) However, such situation need not be realized, for the vortices and the spirals might be fore-and-aft symmetric and the pressure drag would then be much smaller than the previous estimate. Whether or not this is actually the case cannot be decided without more quantitative analysis or computations.

Finally we mention a second alternative model, which is in a sense the opposite extreme of the previous model. As sketched in figure 10(*b*), the contrarotating vortices might be much larger than the jet, which would then be a thin layer normal to the wind in the low-velocity region around the frontal stagnation point of the

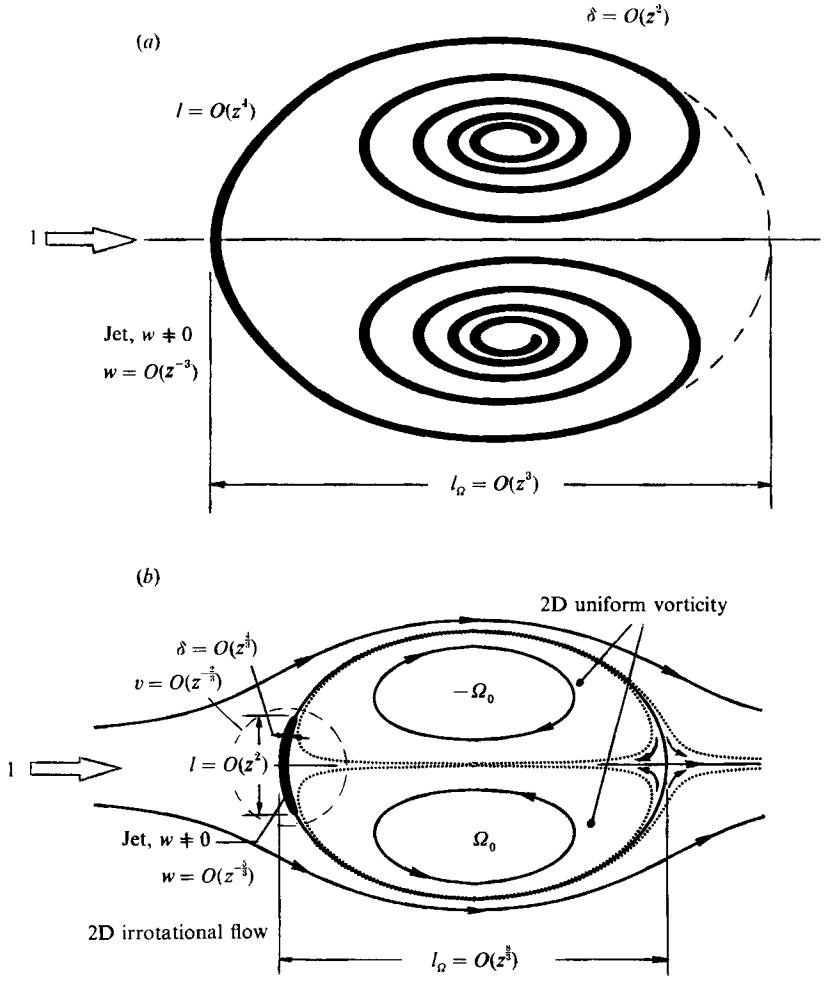

FIGURE 10. Two alternative structures of the jet cross-section for large z.

vortex pair. Calling $v \ll 1$ the characteristic horizontal velocity in this region, the estimate (ii) of §5 should be modified to $w/z \sim v/l$, whereas (i) and (iii) still hold. The actual transfer of momentum from the wind to the jet would be due to the pressure difference between both sides of the layer ($\Delta p = O(v^2)$) rather than to the momentum entrained directly with the surrounding fluid (because $v \ll 1$). The overall horizontal momentum balance for the flow outside the jet now yields the relation $lv^2 \sim m_e$ (the defect of horizontal momentum in the wake is again negligible), which can be combined with the estimates (i)–(iii) to obtain

$$l = O(z^2), \quad \delta = O(z^{\frac{4}{3}}), \quad w = O(1/z^{\frac{5}{3}}), \quad v = O(1/z^{\frac{2}{3}}), \tag{A 3}$$

whereas the downwind shift (obtained as in §5 but with the pressure drag taking the place of the entrainment of horizontal momentum flux) is $x_0 = O(z^{\frac{8}{3}})$, and the size of the contrarotating vortices is $l_\Omega = O(l/v) = O(z^{\frac{8}{3}})$ (because the order of the velocity is expected to grow proportionally to the distance to the stagnation point). Both x_0 and the size of the vortices predicted by this model are smaller than when $v = O(1)$, giving a somewhat better agreement with the numerical results of figures 6 and 8. The main differences with the results of §5 are that the deflection of the jet is now due to

pressure drag and that the height at which the inclination becomes appreciable ($w = O(\beta)$) and three-dimensional effects come into play is $z = O(1/\beta^{\frac{3}{5}})$. A more detailed discussion of this model will be given elsewhere.

REFERENCES

ADLER, D. & BARON, A. 1979 Prediction of a three-dimensional circular turbulent jet in a crossflow. *AIAA J.* **17**, 168–174.

ANDREOPOULOS, J. 1982 Measurements in a jet-pipe flow issuing perpendicularly into a cross stream. *Trans. ASME* I: *J. Fluids Engng* **104**, 493–499.

BATCHELOR, G. K. 1967 *An Introduction to Fluid Dynamics.* Cambridge University Press.

BROADWELL, J. E. & BREIDENTHAL, R. E. 1984 Structure and mixing of a transverse jet in incompressible flow. *J. Fluid Mech.* **148**, 405–412.

CHEN, C. L. H. 1942 Aufrollung eines zylindrischen strahles durch querwind. Doctoral thesis, University of Gottingen.

CHIEN, J. C. & SCHETZ, J. A. 1975 Numerical solution of the three dimensional Navier–Stokes equations with applications to channel flows and a buoyant jet in a cross flow. *Trans. ASME* E: *J. Appl. Mech.* **42**, 575–579.

COELHO, S. L. V. & HUNT, J. C. R. 1989 The dynamics of the near field of strong jets in cross-flows. *J. Fluid Mech.* **200**, 95–120.

CRIGHTON, D. G. & GASTER, M. 1976 Stability of slowly diverging jet flow. *J. Fluid Mech.* **77**, 397–413.

DEMUREN, A. O. 1983 False diffusion in three-dimensional steady flow calculations. *Rep.* SFB 80/T/224. Sonderforschungsbereich 80, University of Karlsruhe.

DURANDO, N. A. 1971 Vortices induced in a jet by a subsonic cross flow. *AIAA J.* **9**, 325–327.

ENDO, H. 1974 A working hypothesis for predicting the path and induced velocity of a jet exhausting at a large angle into a uniform cross-flow. *Trans. Japan Soc. Aero. Space Sci.* **17**, 45–64.

FEARN, R. & WESTON, R. P. 1974 Vorticity associated with a jet in a cross flow. *AIAA J.* **12**, 1666–1671.

HOULT, D. P. & WEIL, J. C. 1972 Turbulent plume in a laminar cross flow. *Atmos. Environ.* **6**, 513–531.

JORDINSON, R. 1958 Flow in a jet directed normal to the wind. *Aero. Res. Council, R. and M.* 3074.

KAMOTANI, Y. & GREBER, I. 1972 Experiments on a turbulent jet in a cross flow. *AIAA J.* **10**, 1425–1429.

KARAGOZIAN, A. R. 1986 An analytical model for the vorticity associated with a transverse jet. *AIAA J.* **24**, 429–436.

KEFFER, J. F. & BAINES, W. D. 1963 The round turbulent jet in a cross wind. *J. Fluid Mech.* **15**, 481–496.

LEGRIVES, E. 1978 Mixing process induced by the vorticity associated with the penetration of a jet into a cross flow. *Trans. ASME* A: *J. Engng Power* **100**, 465–475.

MORRIS, P. J. 1976 The spatial viscous instability of axisymmetric jets. *J. Fluid Mech.* **77**, 511–529.

MOUSSA, Z. M., TRISCHKA, J. W. & ESKINAZI, S. 1977 The near field in the mixing of a round jet with a cross-stream. *J. Fluid Mech.* **80**, 49–80.

NEEDHAM, D. J., RILEY, N., LYTTON, C. C. & SMITH, J. H. B. 1990 A jet in crossflow. Part 2. *J. Fluid Mech.* **211**, 515–528.

NEEDHAM, D. J., RILEY, N. & SMITH, J. H. B. 1988 A jet in crossflow. *J. Fluid Mech.* **188**, 159–184.

PATANKAR, S. V., BASU, D. K. & ALPAY, S. A. 1977 Prediction of the three-dimensional velocity field of a deflected turbulent jet. *Trans. ASME* I: *J. Fluids Engng* **99**, 758–762.

PIERREHUMBERT, R. T. 1980 A family of steady, translating vortex pairs with distributed vorticity. *J. Fluid Mech.* **99**, 129–144.

PLASCHKO, P. 1979 Helical instabilities of slowly divergent jets. *J. Fluid Mech.* **92**, 209–215.

PLATTEN, J. L. & KEFFER, J. F. 1968 Entrainment in deflected axisymmetric jets at various angles to the stream. *Rep.* TP 6808. University of Toronto.

PRATTE, B. D. & BAINES, W. D. 1967 Profiles of the round turbulent jet in a cross flow. *J. Hydraul. Div. Proc. ASCE* **93** (*HY6*), 53–64.

SAFFMAN, P. G. & TANVEER, S. 1982 The touching pair of equal and opposite uniform vortices. *Phys. Fluids* **25**, 1929–1930.

SUCEC, J. & BOWLEY, W. W. 1976 Prediction of the trajectory of a turbulent jet injected into a crossflowing stream. *Trans. ASME* I: *J. Fluids Engng* **98**, 667–673.

SYKES, R. I., LEWELLEN, W. S. & PARKER, S. F. 1986 On the vorticity dynamics of a turbulent jet in a crossflow. *J. Fluid Mech.* **168**, 393–413.

VIZEL, Y. M. & MOSTINSKII, I. L. 1965 Deflection of a jet injected into a stream. *Fluid Dyn.* **8**, 127–139.

WERLÉ, H. 1974 Hydrodynamic visualization of a jet in a crossflow. *ONERA Publication* 156.

WERLÉ, H. 1990 Hydrodynamic visualization of separated flows and jets. *ONERA Publication* 4271.